JOURNAL OF
HYDRO-METEOROLOGY

Rerearch Article

Efficient oil removal from water using carbonized rambutan peel: Isotherm and kinetic studies

Trinh Trong Nguyen[1,2], Nguyen Dinh Loc[1], Le Huy Ba[2], Thai Van Nam[1]*

[1] HUTECH Institute of Applied Sciences, HUTECH University, 475A Dien Bien Phu Street, Ward 25, Binh Thanh District, Ho Chi Minh City 700000, Vietnam; tt.nguyen@hutech.edu.vn; 6009220001@hufi.edu.vn; lochenni@gmail.com; tv.nam@hutech.edu.vn

[2] Ho Chi Minh City University of Industry and Trade, 140 Le Trong Tan Street, Tay Thanh Ward, Tan Phu District, Ho Chi Minh City 700000, Vietnam; tt.nguyen@hutech.edu.vn; 6009220001@hufi.edu.vn; lhuyba@gmail.com

*Corresponding author: tv.nam@hutech.edu.vn; Tel: +84–945007990

Received: 08 September 2023; Accepted: 02 October 2023; Published; 25 December 2023

Abstract: The study aims to assess the diesel oil adsorption capacity of activated carbon derived from rambutan peel, a prevalent agricultural by-product in Vietnam. The adsorption process will be investigated using various adsorption isotherms (Langmuir, Freundlich, Temkin, Dubin-Radushkevich), adsorption kinetics (pseudo-first order and pseudo-second order). The characterization analysis of RPAC revealed the following values: BET surface area of 786.0143 m^2/g, BJH adsorption cumulative volume of pores at 0.05392 cm^3/g, and BJH adsorption average pore diameter of 55.2432 nm. Individual assessments of factors influencing oil removal efficiency and adsorption capacity identified the optimal initial oil concentration at 1% volume/volume, an optimum contact time of 60 minutes, and an equilibrium adsorption time of 80 minutes. The optimal adsorbent dosage was 250 mg, and the ideal pH was 6. The adsorption process adhered to the Langmuir isotherm with an R^2 value of 0.9993, yielding a maximum adsorption capacity of 5,712.0 mg/g. The pseudo-second-order model provided a better fit for RPAC's oil adsorption process with an R^2 value of 0.9969.

Keywords: Activated carbon; Diesel oil; Materials science; Modeling; Rambutan peel.

1. Introduction

The total volume of oil released into the environment from oil tanker spills in 2021 was approximately 10,000 tons [1]. Oil-polluted wastewater affects water quality and underwater ecosystems worldwide [2], posing severe health consequences [3].

Methods for oil removal in water can be categorized into in-situ burning, chemical methods (solidification, dispersion), biological methods, and physical methods (skimming, adsorbents) [4]. Among these, oil adsorbents remain the preferred technique for oil clean-up due to their speed, simplicity, environmental friendliness [5], and cost-effectiveness. The choice of adsorbent material depends on factors such as availability, cost, and safety considerations [6]. Currently, about 200 different types of adsorbent materials are being produced and used [6], classified into three main groups: inorganic minerals, synthetic organic products, and natural organic products [7]. Among these, adsorbent materials of natural organic origin offer significant advantages compared to others, especially in terms of environmental friendliness in marine environments and their lightweight nature, making them easily recoverable and reusable [8].

Activated carbon, derived from carbonization, is used for adsorbing various compounds [9–10]. Activated carbon from plant biomass is particularly favored due to its abundant and readily available source, resulting in significantly lower production costs compared to commercial activated carbon [11]. Consequently, many different activated carbon materials have been synthesized from various plant-based sources, such as coconut shells [11], coconut coir [12], safou seeds [13], corn cobs [10, 14], rice husks [15, 16], and barley straw [17].

According to the General Statistics Office data, Vietnam's total agricultural by-products in 2020 amounted to over 156.8 million tons, with 88.9 million tons of post-harvest by-products from crops and agricultural processing (accounting for 56.7%) [18]. The current challenge is effectively utilizing and recycling agricultural residues to support farmers' livelihoods while minimizing environmental impact. Among these residues, those with high lignocellulose content present an important area of research for selecting suitable agricultural by-products to fabricate efficient and cost-effective oil-adsorbent materials. Rambutan belongs to the 10 main fruit-bearing trees group in Vietnam [19]. Rambutan peel (RP) is an agricultural waste with a high cellulose content, constituting approximately 24.28% [20]. Cellulose is a crucial structural component of adsorbent materials [21], capable of enhancing the oil recovery efficiency of these materials in aqueous environments [22]. Consequently, RP is considered a cost-effective and suitable adsorbent material for oil removal in water. Numerous studies have demonstrated the potential of using activated carbon derived from rambutan peel for the removal of Fe(II) from aqueous solutions [23] and the removal of Remazol Brilliant Blue R [24].

This study aimed to investigate the individual effects of factors influencing RP's oil removal efficiency and adsorption capacity, followed by conducting isotherm and kinetic studies on the adsorption process.

2. Material and methods

The research diagram is presented in Figure 1.

2.1. Materials

Rambutan peel was sourced from the main market in HCMC, Vietnam, and the rambutan variety used is Dona rambutan. The diesel oil (DO) 0.05S was obtained from Petrolimex Aviation in HCM, Vietnam, with a specific gravity at 15^{o}C of 820-860 kg/m^{3}. Potassium hydroxide, n-Hexane, and sodium sulfate anhydrous were sourced from Xilong Scientific Co., Ltd. in Shenzhen, China. Sulfuric acid (c(H_2SO_4) = 0.05 mol/l or 0.1 N) for a 1000 ml solution and hydrochloric acid (c(HCl) = 0.1 mol/l or 0.1 N) were provided by Merck in Germany.

2.2. Preparation of adsorbent and simulated oil spill

Rambutan peel underwent rinsing with tap water, subsequent drying at 105^{o}C for 24 hours to eliminate moisture, grinding, and sieving to achieve a particle size of 1-2 mm. The resulting dried RP was introduced into a stainless steel vertical tubular reactor positioned within a tube furnace. Carbonization was executed at 550^{o}C for a duration of 2 hours in an environment of purified nitrogen (99.99%). The resulting product, rambutan peel char (RPC), was subsequently combined with KOH pellets at a 1:2 impregnation ratio [24]. Deionized water was added to dissolve the entire KOH pellets, resulting in a KOH concentration of 1M, and the mixture was soaked for 24 hours. The mixture was dried in an oven at 105^{o}C for 24 hours to remove moisture and then subjected to activation in a muffle furnace at 550^{o}C for 1 hour. The resulting rambutan peel activated carbon (RPAC) was subsequently cooled, treated with a 0.1 M HCl solution to eliminate ash content, and rinsed with distilled water until the pH of the washing solution stabilized at 6-7. The prepared RPAC was dried in an oven at 105^{o}C for 2 hours, crushed, and sieved into various particle sizes before being stored in a

desiccator for use in the next experiment. The simulated oil-water mixture was prepared by mixing 2.5 mL of DO with 250 mL water in a beacher of 250 ml of brine water (1.0% volume/volume).

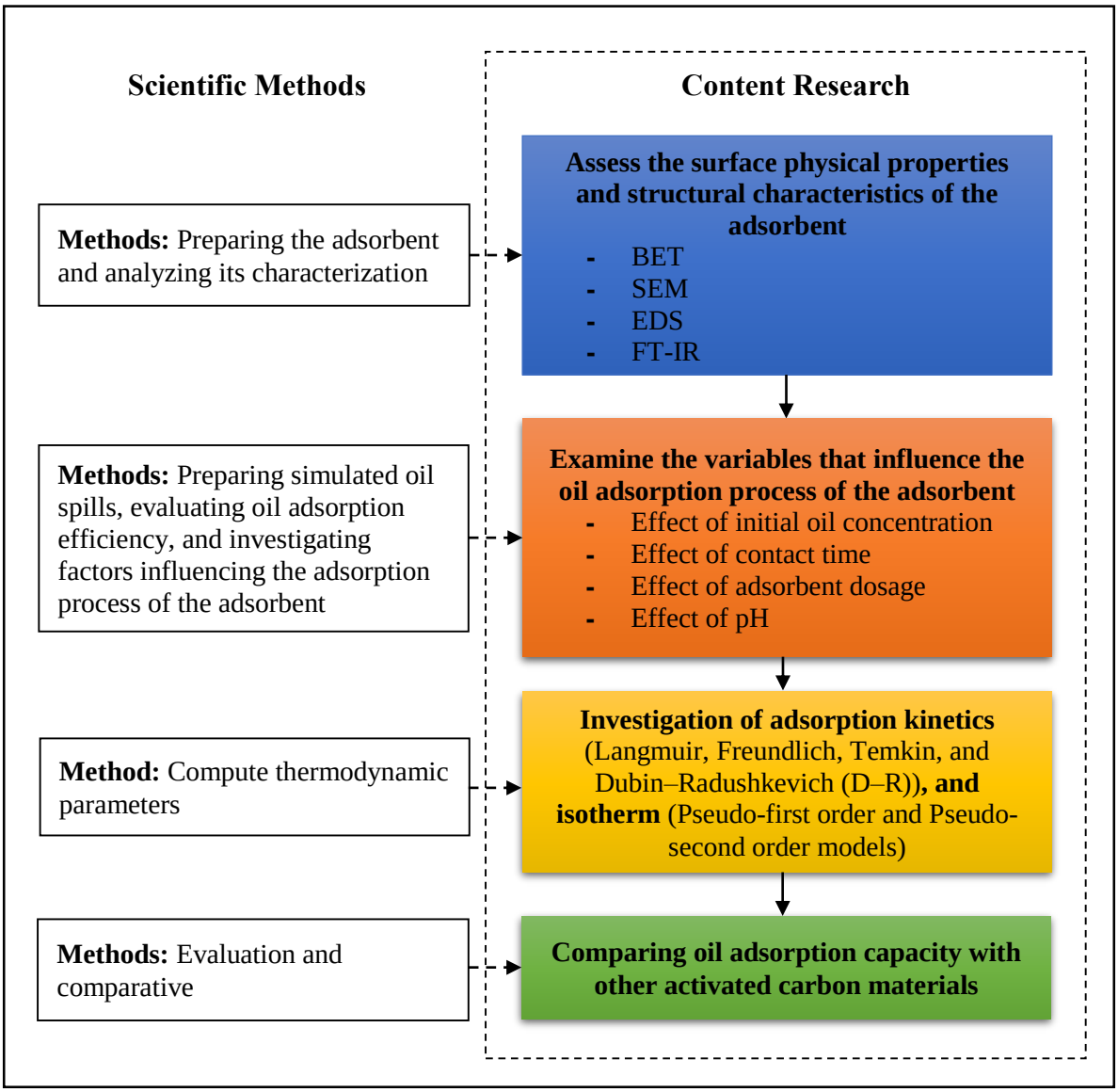

Figure 1. Research diagram.

2.3. Characterization of adsorbent

The surface area, pore volume, and average pore diameter of the RPAC prepared under optimal conditions were assessed using the Micromeritics® TriStar II Plus Version 3.03. Scanning Electron Microscope (SEM) and Energy Dispersive X-ray Spectroscopy (EDS) analyses were performed with the JSM-IT500 InTouchScope™ Scanning Electron Microscope. Fourier-transform infrared spectroscopy (FT-IR) measurements were conducted using the Agilent Cary 630 FTIR spectrometer.

2.4. Method to evaluate the efficiency of oil adsorption

For each experiment, the amount of adsorbed oil per gram of adsorbent at equilibrium is denoted as q_e (mg/g), at time t is q_t (mg/g), and the adsorption efficiency is determined using the following formula [24]:

$$q_e = \frac{(C_o - C_e) * V}{M} \quad (1)$$

$$q_t = \frac{(C_o - C_t) * V}{M} \quad (2)$$

$$\%\, Effective\ removal = \frac{(C_o - C_e) * 100}{C_o} \quad (3)$$

where C_o is the initial oil concentration (mg/L), C_e is the equilibrium concentration (mg/L), C_t is the oil concentration at time t (mg/L), V is the volume of the solution (ml), and M is the mass of the adsorbent used (mg).

2.5. Investigating the factors affecting the oil adsorption process of the adsorbent

The factors affecting the oil adsorption process of the adsorbent will be sequentially investigated from Experiments 1 to 4. The optimized values obtained from each experiment will be utilized for the subsequent experiment. The experimental layout is presented in Table 1.

Table 1. Experiment to investigate the factors affecting the oil adsorption process.

Experiment	Initial oil concentration (% v/v)	Contact time (min)	Adsorbent dosage (mg)	pH	Adsorbent particle size (mm)	Temperature (ºC)
Experiment 1: Investigating the effect of initial oil concentration	Range 0.25 - 2 (jump interval 0.25)	60	250	7 ± 0.2	0.6 ÷ 1.0	25 ± 1
Experiment 2: Investigating the impact of contact time	Optimization of Experiment 1	Range 10 - 90 (jump interval 10)	250	7 ± 0.2	0.6 ÷ 1.0	25 ± 1
Experiment 3: Investigating the influence of adsorbent dosage	Optimization of Experiment 1	Optimization of Experiment 2	Range 250 - 1,500 (jump interval 250)	7 ± 0.2	0.6 ÷ 1.0	25 ± 1
Experiment 4: Investigating the effect of pH	Optimization of Experiment 1	Optimization of Experiment 2	Optimization of Experiment 3	Range 3 - 11 (jump interval 1)	0.6 ÷ 1.0	25 ± 1

2.6. Sorption Isotherms and Kinetics

In this study, four commonly used sorption isotherm models, namely Langmuir (4), Freundlich (5), Temkin (6), and Dubin–Radushkevich (D–R) (7) equations, were used to fit the experimental data [25]:

$$\frac{C_e}{q_e} = \frac{C_e}{q_{max}} + \frac{1}{q_{max} K_L} \quad (4)$$

$$\ln q_e = \ln K_f + \frac{1}{n} \ln C_e \quad (5)$$

$$q_e = B_T \ln K_T + B_T \ln C_e \quad (6)$$

$$\ln q_e = \ln q_{D-R} - K_{ad} \varepsilon^2 \quad (7)$$

where C_e is the equilibrium concentration of adsorbate (mg/L), q_e is the amount of oil adsorbed per gram of the adsorbent at equilibrium (mg/g), q_{max} is the maximum monolayer adsorption capacity (mg/g), K_L is Langmuir isotherm constant (L/mg), K_f is Freundlich isotherm constant (mg/g), n is adsorption intensity, B_T is constant related to heat of sorption(J/mol), K_T is Temkin isotherm equilibrium binding constant (L/g), q_{D-R} is theoretical

isotherm saturation capacity (mg/g), K_{ad} is Dubinin-Radushkevich isotherm constant (mol^2/kJ^2), and ε is Polanyi potential.

First-order and pseudo-first-order kinetic model [26] and Second-order and pseudo-second-order kinetic model [27] are presented in equations (8) and (9).

$$log(q_e - q_t) = log(q_e) - \frac{k_1}{2.303}t \quad (8)$$

$$\frac{t}{q_t} = \frac{1}{k_2 q_e^2} + \frac{1}{q_e}t \quad (9)$$

where q_t and q_e are the amount of oil sorbed per mass of sorbent (mg/g) at time t (min) and equilibrium, respectively. k_1 (1/min) and k_2 (g/mg.min) are the constant rate parameters of the pseudo-first-order and the pseudo-second-order sorption, and h (mg/g.min) is the initial sorption rate.

3. Results and discussion

3.1. Characteristics of the adsorbent

3.1.1. Surface physical characteristics of the adsorbent

Surface physical characteristics of RPC and RPAC were determined using Brunauer-Emmett-Teller (BET) analysis and are presented in Table 2.

Table 2. Surface physical characteristics of RPC and RPAC.

Surface physical characteristics	RPC	RPAC
BET surface area (m^2/g)	485.7680	786.0143
BJH adsorption cumulative surface area of pores (m^2/g)	0.9787	10.3904
BJH adsorption cumulative volume of pores (cm^3/g)	0.005293	0.05392
BJH adsorption average pore diameter (nm)	21.6336	55.2432

The adsorbents' pore properties and surface area were determined using BET isotherm analysis. The BET surface area of RPC and RPAC were 485.7680 (m^2/g) and 786.0143 (m^2/g), respectively. The increased BET surface area in RPAC indicated more active sites, enhancing oil uptake [28]. Compared to other naturally derived organic materials that have undergone carbonization, such as coconut coir (with a surface area of 691.800 m^2/g) [12] and plantain peels fiber (with a surface area of 234.51 m^2/g) [28], the surface area of RPAC is higher.

The pore volume increased from 0.005293 to 0.05392 (cm^3/g), while the pore diameter increased from 21.6336 to 55.2432 nm. The average pore diameter of RPAC (55.2432 nm) is higher than the average pore size of activated carbon from corncobs (45 nm) [10], rambutan peel-based activated carbon (2.63 nm) [24], and carbonized plantain peels fiber (4.77 nm) [28].

From these findings, it is evident that RPAC exhibits larger surface area, total pore volume, and pore diameter in comparison to RPC. This creates advantageous circumstances for the adsorption process to occur on the adsorbent's surface, consequently augmenting RPAC's oil retention and adsorption capacity. The enhancement in BET surface area can likewise be ascribed to the removal of volatile organics during thermal treatment [29]. The enhanced pore characteristics will facilitate the diffusion of a greater number of oil molecules onto the RPAC surface [28, 30].

3.1.2. Surface and structural characteristics of the adsorbent

The SEM images depicting the surface and structural characteristics of raw RP, RPC, and RPAC at ×1,000 magnification are presented in Figure 2.

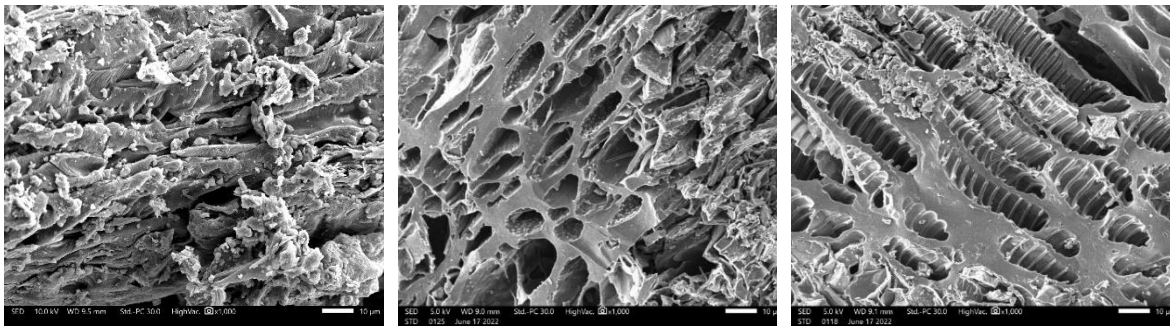

a) b) c)

Figure 2. SEM images (×1,000) of raw RP (a), RPC (b), and RPAC (c).

Based on the SEM images at ×1,000 magnification, the surface structure of raw RP displays uniform fiber-like crystal bonds and small pores, indicating the presence of minerals (Figure 2a). The surface mainly comprises a lignocellulose network and fiber matrix containing lignin, cellulose, volatile organic compounds, and hemicellulose. After carbonization, RPC's surface exhibits uneven, rough, and rugged structures with numerous existing pores (Figure 2b). Alkaline treatment results in larger, deeper pores, increasing their number on the material's surface (Figure 2c). The KOH-C reaction enhances pore development during activation, thereby increasing surface area and adsorption capacity. A nearly heterogeneous pore structure pattern is also observed on the RPAC surface.

The immersion of activated carbon in KOH solution enhances the adsorption activity of the adsorbent by creating potassium carbonate crystals on the carbon surface. These crystals generate airflow holes on the surface of adsorbents, boosting adsorption capacity and increasing the existing surface area for adsorbing organic compounds, including oil from water, during adsorption. Furthermore, the immersion process also forms active functional groups on the carbon surface, playing a vital role in adsorbing organic substances.

The observed formation of pores on the surface of RPAC material aligns with findings by [24] regarding rambutan peel activation and with the study by [12] on activated carbon production from coconut coir.

3.1.3. FT-IR analysis of the adsorbent

The analysis of raw RP and RPAC samples using FT-IR spectra revealed the presence of various peaks, indicative of distinct functional groups, across the wavelength range of 650 - 4000 cm^{-1}, as depicted in Figures 3 and 4.

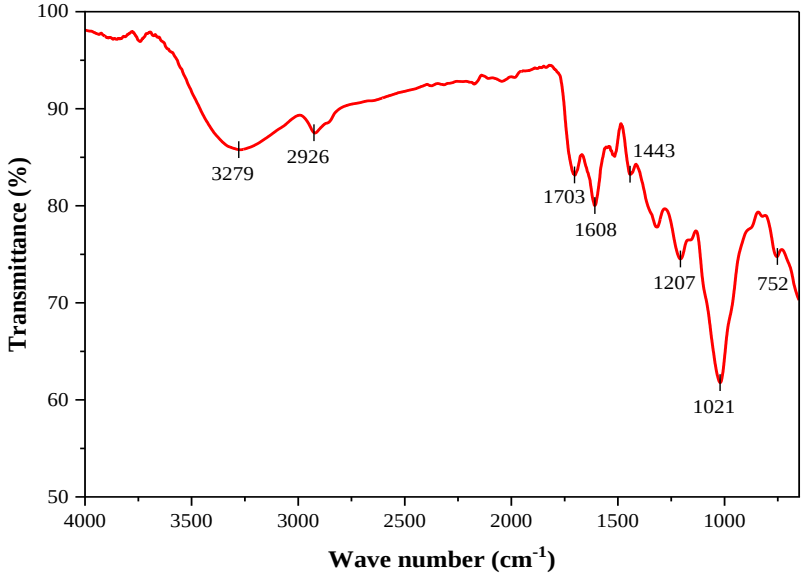

Figure 3. FT-IR of raw RP.

The FT-IR spectrum of rambutan peel reveals distinct functional groups. A peak at 3279 cm^{-1} signifies the presence of (O-H) groups, originating from alcohol and carboxylic acid moieties. Furthermore, an aliphatic C-H group is evident at 2926 cm^{-1}. Notably, a non-ionic carbonyl group (C=O) is identified at 1703 cm^{-1}. Other significant peaks include 1608 cm^{-1}, representing a -COO-carboxylate group, 1443 cm^{-1}, signifying a symmetrical carboxylate group, and 1207 cm^{-1}, indicating a C-O group derived from ether (resulting from lignin bonding with cellulose). These findings align with previous studies [31] regarding the functional group characteristics of rambutan peel. Additionally, the band at 1021 cm^{-1} is attributed to C-OH [32], while at 752 cm^{-1}, the presence of Methylene—$(CH_2)_n$—rocking ($n \geq 3$) is observed [33]. This comprehensive characterization enhances our understanding of the chemical composition of rambutan peel.

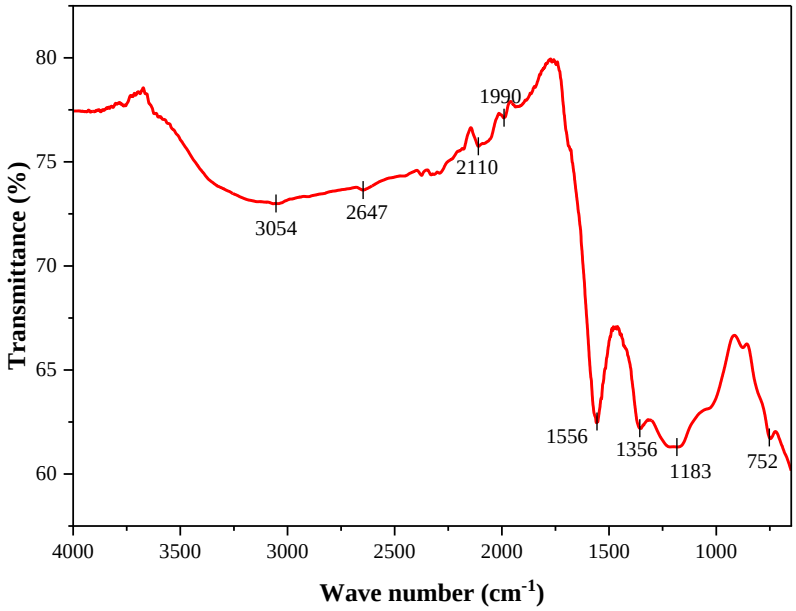

Figure 4. FT-IR of RPAC.

For RPAC, at 3054 cm^{-1}, we observe a distinct C-H stretching indicative of an alkene group. The presence of a carboxylic acid group is evident at 2647 cm^{-1}, characterized by its -OH stretching. Additionally, the spectrum features a sharp peak at 2110 cm^{-1}, corresponding to the C≡C stretching of an alkyne group [12]. At 1990 cm^{-1}, we discern a C-H bending pattern, which is characteristic of an aromatic compound. Furthermore, the spectrum highlights several important peaks: at 1556 cm^{-1}, there is a pronounced C=C stretching, characteristic of an aromatic benzene ring group [12]. At 1356 cm^{-1}, we observe an O-H bending pattern, indicative of phenol. Lastly, at 1183 cm^{-1}, there is a distinct C-O stretching signal associated with a tertiary alcohol group. In addition to these functional group vibrations, the presence of methylene groups is clearly detected at 752 cm^{-1}, where the Methylene —$(CH_2)_n$—rocking ($n \geq 3$) motion is observed [33].

Both raw RP and RPAC exhibit the presence of various functional groups, as depicted by distinct FT-IR spectral peaks at different wavenumbers. These functional groups include C-H, -OH, -COO, and Methylene—$(CH_2)_n$—rocking ($n \geq 3$), and they appear in both samples, albeit at different positions and intensities. However, significant differences also exist, such as the presence of a non-ionic carbonyl group (C=O) and a -COO-carboxylate group in raw RP but not in RPAC. Conversely, RPAC displays features like C≡C stretching of an alkyne group and C=C stretching of an aromatic benzene ring group that are absent in raw RP. Moreover, each sample's FT-IR spectrum exhibits distinctive spectral peaks, aiding in the identification of their specific chemical compositions and properties. The results of the

EDX analysis will further specify the exact concentrations of substances within the adsorbent material.

3.1.4. EDS analysis

The results of EDS analysis of the raw RP and RPAC are shown in Table 3 and Figures 5 and 6.

Table 3. Result of EDS analysis of raw RP and RPAC.

Elements	Raw RP	RPAC
Carbon (C)	64.1	79.8
Oxygen (O)	35.9	15.9
Nitrogen (N)	0.0	0.0
Potassium (K)	0.0	4.3
Toatl (wt%)	100.0	100.0

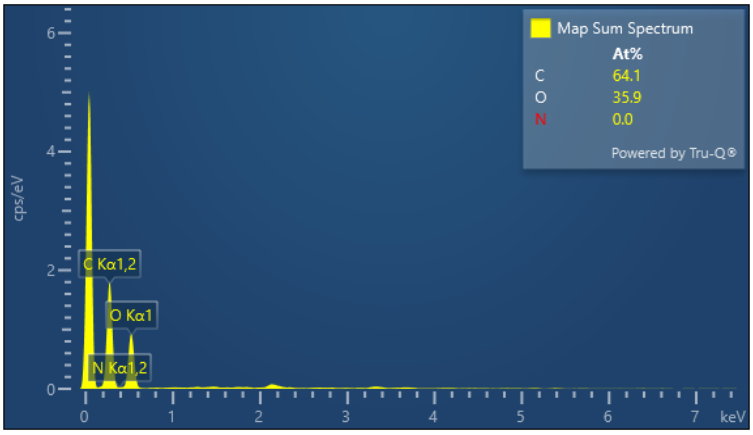

Figure 5. EDS spectrum of raw RP.

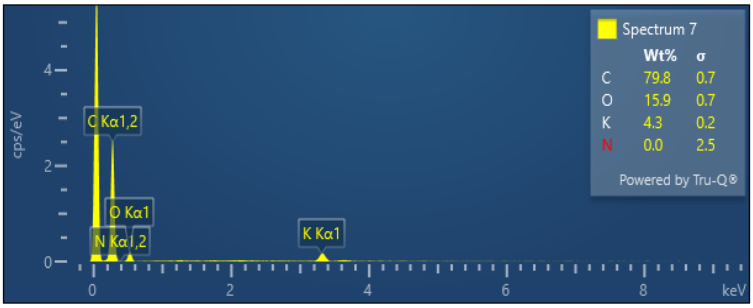

Figure 6. EDS spectrum of RPAC.

The EDS analysis revealed that carbon is the predominant component in both raw RP and RPAC. The carbon content in raw RP is 64.1 wt%, accompanied by an oxygen content of 35.9 wt%. In the case of RPAC, the carbon content increases to 79.8 wt%, while the oxygen content decreases to 15.9 wt%. Notably, there is also a presence of potassium (K) at 4.3 wt% in RPAC. The appearance of K in RPAC results from the treatment of raw RP with KOH during the activation process aimed at producing activated carbon. The levels of C, O and K in RPAC closely resemble those found in activated carbon derived from durian shells [34]. According to the Indonesian Standard SNI 06-3730-1995, the minimum required pure carbon component for activated carbon is 65% [35]. In this experiment, nearly 80% of the composition in RPAC consists of carbon, thus meeting the requirements of the Indonesian Standard (SNI). The high carbon content in rambutan peel can be attributed to its substantial

lignocellulose component. These findings highlight the potential of rambutan peel as a promising raw material for activated carbon production.

3.2. Factors influencing the batch adsorption equilibrium investigations

The batch adsorption equilibrium experiments concerning the adsorption of oil onto RPAC yielded the following results:

3.2.1. Effect of initial oil concentration and isotherm studies

Studying initial oil concentration is crucial due to its strong influence on the thermodynamics and kinetics of the adsorption process [36]. The results of investigating the impact of initial oil concentration on RPAC's oil adsorption capacity and removal efficiency are presented in Figure 7.

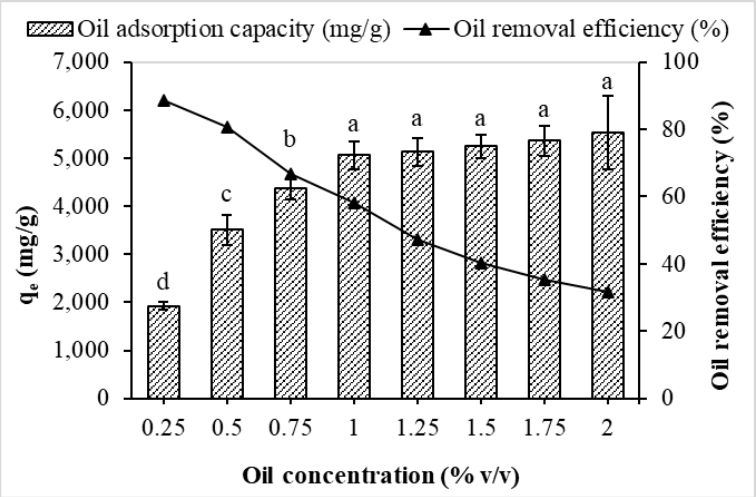

Figure 7. Effect of initial oil concentration on oil adsorption capacity and removal efficiency (Experimental conditions: adsorbent particle size = 0.6 - 1.0, adsorbent dosage = 250 mg per 250 ml of oil-contaminated water, temperature = 25 ± 1°C, contact time = 60 min, pH = 7 ± 0.2, and initial oil concentration = 0.25 - 2.0 % v/v). The error bars represent the mean (SD) for three replicates (n = 3).

At an initial oil concentration of 0.25% v/v, the removal efficiency reached 88.57%. However, this ratio decreased to 31.76% as the initial oil concentration increased to 2% v/v. This decrease in removal efficiency at higher initial concentrations (for the same adsorbent dosage) can be attributed to the reduction in the number of available active sites on the adsorbent's surface responsible for oil binding. This finding aligns with Abel et al. (2020) [12], who observed a similar trend when using coconut coir-activated carbon to remediate oil spills.

The adsorption capacity of the adsorbent increases with higher initial oil concentrations, particularly in the range of initial oil concentrations from 0.25% v/v (1,926.3 mg/g) to 1% v/v (5,064.3 mg/g). This is attributed to the higher ratio of surface active sites on the adsorbent to oil molecules at low initial concentrations (0.25% v/v), causing more oil molecules to interact with the adsorbent and occupy the active sites on its surface. As the initial oil concentration exceeds 1% v/v, oil molecules rapidly occupy the surface active sites of the adsorbent, leading to early saturation. The limited number of active sites available on the adsorbent's surface for oil molecules results in a gradual reduction in removal efficiency. Consequently, the adsorption capacity of the adsorbent only slightly increases when the initial oil concentration shifts from 1% v/v (5,064.3 mg/g) to 2% v/v (5,526.9 mg/g). This finding aligns with experimental data from Cheu et al. (2016), indicating that oil adsorption capacity increases with oil concentration until reaching a certain threshold and reaching

equilibrium. This result is attributed to the saturation of active sites on the adsorbent's surface with oil, hindering further oil adsorption onto these active sites [37].

The ANOVA results indicate significant differences in RPAC's oil adsorption capacity between the initial oil concentration of 1% v/v and the concentrations of 0.25, 0.5, and 0.75% v/v. However, no substantial distinctions were found among the higher initial oil concentrations and 1% v/v. Within the scope of this study, the authors will select the optimal initial oil concentration of 1% v/v to investigate the impact of contact time on RPAC's oil adsorption process.

Based on the initial oil concentration study, the calculated isotherms of Langmuir, Freundlich, Temkin, and Dubin-Radushkevich (D-R) are presented in Figure 8.

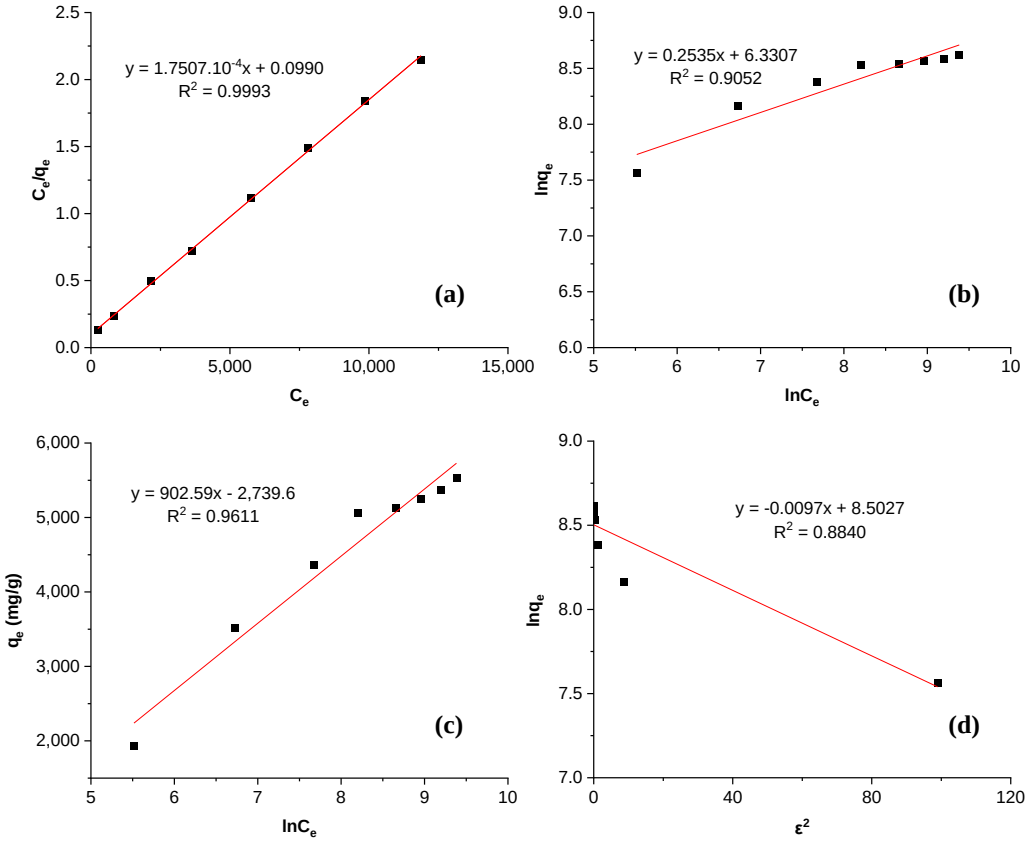

Figure 8. Equilibrium isotherms for oil adsorption onto prepared RPAC: (a) Langmuir, (b) Freundlich, (c) Temkin, and (d) Dubin-Radushkevich isotherms.

Table 4. Parameters and correlation coefficients for various isotherm models in sorption study.

Isotherm	Parameter	Calculated value
Langmuir	q_{max} (mg/g)	5,712.0
	K_L (L/mg)	0.0018
	R^2	0.9993
Freundlich	K_f (mg/g)	561.55
	1/n	0.2535
	R^2	0.9052
Temkin	K_T (L/g)	0.0481
	B (J/mol)	902.59
	b_T	2.7463
	R^2	0.9611
D-R	Q_{D-R} (mg/g)	4,928.1
	K_{ad} (mol^2/KJ^2)	0.0097
	E (KJ/mol)	7.1796
	R^2	0.8840

The calculated isotherms results reveal that the Langmuir isotherm exhibits a higher coefficient R^2 (0.9993) compared to other sorption isotherm models. This implies that the Langmuir isotherm is the most suitable model for describing RPAC's oil adsorption process under the conditions of this study. These results demonstrate that the oil adsorption process on RPAC can be explained using a monolayer adsorption model with consistent conditions for all active sites on RPAC's surface. Accordingly, RPAC's adsorption capacity saturates when all surface active sites are filled with oil molecules. The Langmuir model indicates that as the oil concentration increases, RPAC's adsorption capacity rises and reaches a maximum value (q_{max}) at a certain point. Subsequently, as the initial oil concentration continues to increase, RPAC's adsorption capacity doesn't increase significantly and gradually reaches a stable value. This aligns with the experimental results presented in Figure 7 of this study.

Additionally, the Langmuir isotherm model also shows that RPAC's adsorption process is physical adsorption. This can be explained by the property of RPAC that the existence of pores on the surface. These pores can physically interact with oil molecules through the Van der Waals force.

The Langmuir isotherm model allows the computation of RPAC's maximum adsorption capacity. This can aid in assessing RPAC's effectiveness in oil removal and its practical applications. Accordingly, the maximum adsorption capacity (q_{max}) of RPAC is 5,712.0 mg/g, and the Langmuir constant (K_L) is 0.0018 L/mg.

3.2.2. Effect of contact time on oil sorption and kinetics studies

Adsorption is a process that varies with time, and it is crucial to understand the adsorption rate for designing and assessing the efficiency of adsorbents in oil removal [38]. The influence of contact time on the oil adsorption capacity and oil removal effectiveness of RPAC was investigated within the range of 10 to 90 minutes, and the results are shown in Figure 9.

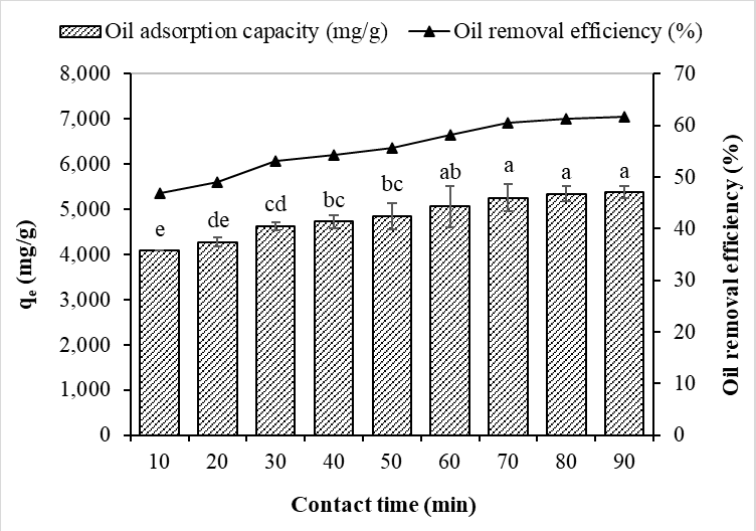

Figure 9. Effect of contact time on oil adsorption capacity and removal efficiency (Experimental conditions: adsorbent particle size = 0.6 - 1.0, adsorbent dosage = 250 mg per 250 ml of oil-contaminated water, temperature = 25 ± 1°C, pH = 7 ± 0.2, and initial oil concentration = 1.0 % v/v, contact time = 10 - 90 min). The error bars represent the mean (SD) for three replicates (n = 3).

The oil adsorption capacity of RPAC rapidly increases within the first 10 minutes of contact with oil, reaching 4,077.7 mg/g and achieving a removal efficiency of 46.87%. This indicates RPAC's strong affinity for diesel oil. After 10 minutes, the oil adsorption capacity continues to rise gradually, showing a tendency to reach equilibrium at 80 minutes (achieving 5,338.3 mg/g adsorption capacity and 61.36% removal efficiency). This can be explained by the fact that during the initial phase, a significant portion of RPAC's surface active sites

remains unoccupied by oil molecules. Consequently, their adsorption capacity and removal efficiency can increase rapidly. However, as the surface active sites become saturated with oil molecules, competition among these molecules gradually reduces the adsorption rate, ultimately reaching equilibrium. This trend aligns with the findings of Ukpong et al. (2020), where the adsorption of crude oil onto activated carbon from coconut husks was rapid in the initial 15 to 30 minutes of contact, followed by a slower pace before finally achieving saturation after 105 minutes [12].

The ANOVA analysis results indicate no significant difference in oil adsorption capacity at different time intervals beyond 60 minutes of contact. Therefore, a 60-minute contact time was chosen as the optimal duration for conducting experiments to investigate the effect of adsorbent dosage on RPAC's oil adsorption capacity. This finding is consistent with Hussein's study, which compared the adsorption capacity of activated carbon from bagasse with a commercial adsorbent and found the maximum adsorption time to be 60 minutes [39]. Compared to the study by [12], the adsorption time of RPAC in this study is faster than the 105 minutes for activated carbon from coconut husks. This difference is due to the type of oil used in the test. Crude oil has a higher viscosity than diesel oil, so the adsorption time to reach equilibrium is longer [39].

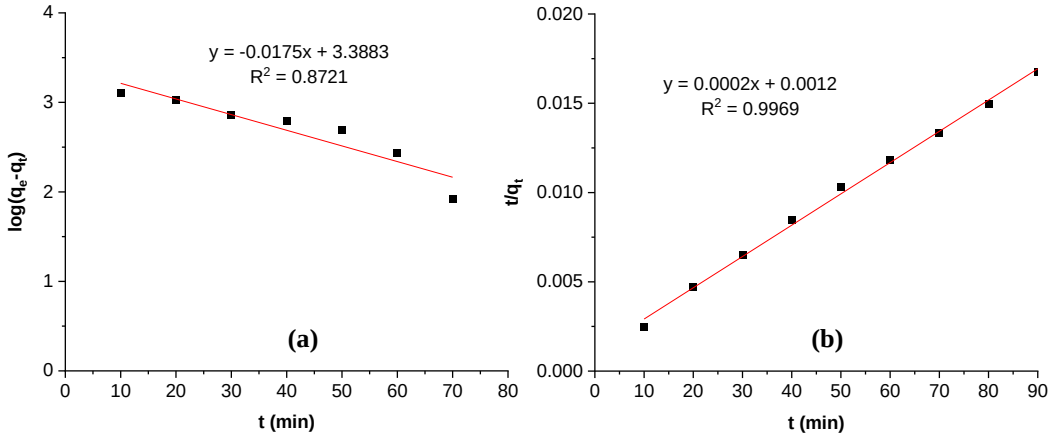

Figure 10. Comparing the (a) pseudo-first-order and (b) pseudo-second-order rate equation models for RPAC.

Table 5. Thermodynamics parameters of crude oil sorption by RPAC for first and second-order models.

$q_{e\ exp}$ (mg/g)	Pseudo-first order			Pseudo-second order			
	$q_{e\ calc}$ (mg/g)	k_1 (1/min)	R^2	$q_{e\ calc}$ (mg/g)	k_2 (g/mg.min)	h (mg/g.min)	R^2
5,338.3	2,445	0.0403	0.8721	5,707	$2.6465.10^{-5}$	862.07	0.9969

where: q_e: the amount of oil adsorbed at equilibrium (mg/g); q_t: the amount of oil adsorbed at time t (mg/g); $q_{e\ exp}$: the experimental adsorption capacity (mg/g); $q_{e\ calc}$: the theoretical adsorption capacity (mg/g).

The calculations based on the Pseudo-first order model yielded an adsorption capacity of 2,445 mg/g, significantly lower than the experimental adsorption capacity of 5,338.3 mg/g. On the other hand, according to the Pseudo-second order model, the theoretical adsorption capacity reached 5,707 mg/g, which closely resembles the experimental adsorption capacity. Additionally, the R-squared value (R^2) of the Pseudo-second order model (R^2 = 0.9969) is higher compared to the Pseudo-first order model (R^2 = 0.8721). Therefore, the Pseudo-second order model (with a rate constant k_2 of $2.6465.10^{-5}$ g/mg.min and a coefficient h of 862.07 mg/g.min) is better suited for describing the oil adsorption process of RPAC under the conditions of this study. The Pseudo-second order model indicates that RPAC's adsorption process exhibits strong adsorption characteristics, particularly at high oil concentrations, and can adsorb a significant amount of oil within a short time frame. This is clearly shown in the

experiment, where RPAC's oil adsorption capacity significantly increases to 4,077.7 mg/g within the first 10 minutes of oil contact. This finding aligns with the research by Anwana Abel et al., where the predominant kinetic model for the adsorption behavior of crude oil on coconut coir-activated carbon was the Pseudo-second order model [12].

3.2.3. Effect of adsorbent dosage

The results of the investigation into the influence of adsorbent dosage are presented in Figure 11.

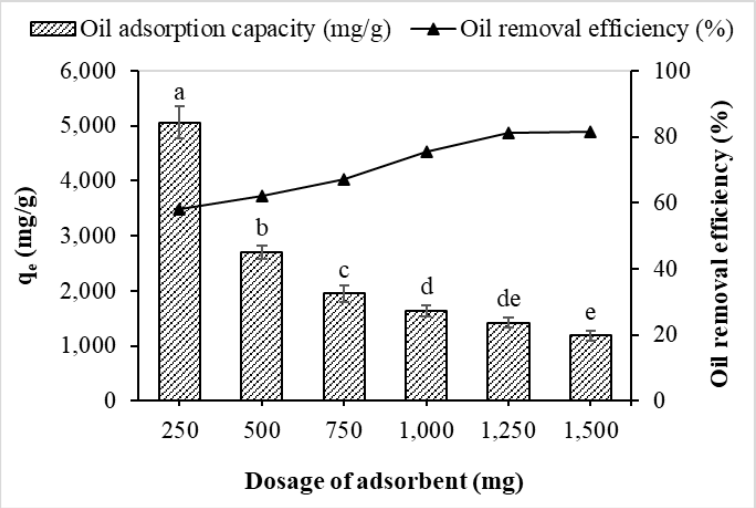

Figure 12. Effect of adsorbent dosage on oil adsorption capacity and removal efficiency (Experimental conditions: adsorbent particle size = 0.6 - 1.0, temperature = 25 ± 1°C, pH = 7 ± 0.2, initial oil concentration = 1.0 % v/v, contact time = 60 min, and adsorbent dosage = 250 - 1,500 mg per 250 ml of oil-contaminated water). The error bars represent the mean (SD) for three replicates (n = 3).

As the dosage of the adsorbent increases from 250 g to 1,500 mg, the oil adsorption capacity rises from 1,266.1 mg to 1,774.6 mg, and the oil removal efficiency increases from 58.21% to 81.59%. This trend can be attributed to the higher availability of active sites on RPAC's surface as the dosage increases, which becomes occupied by oil molecules, resulting in enhanced oil adsorption. This result aligns with the findings [40], who demonstrated that the oil removal percentage of powdered activated lemon peels is directly proportional to the adsorbent dosage. Larger dosages lead to higher oil adsorption efficiency due to the increased surface area for adsorption to occur.

However, at higher dosages in this specific study, such as 1,250 mg (with an oil removal efficiency of 81.34%) and 1,500 mg (with an oil removal efficiency of 81.59%), the removal efficiency nearly plateaus. This could be attributed to an excess of RPAC in the environment, hindering the penetration of oil molecules to occupy active sites on the surface, thus limiting further adsorption capacity and preventing complete oil removal. This phenomenon has also been demonstrated by [41], where the adsorption capacity increased with increasing adsorbent dosage from 500 mg to 1,500 mg, followed by a decreasing trend. This reduction could be due to the compaction of fibers at higher dosages, potentially reducing the even penetration of oil into the fibers. Determining the optimal dosage of adsorbent is crucial as it significantly impacts the capacity and removal efficiency of the oil adsorption process in real-world conditions. This helps save resources, optimize processing efficiency, protect the environment, and reduce costs, while also creating favorable conditions for adsorbent reuse. The calculated oil adsorption capacity per gram of material (q_e) gradually decreases from 5,064.3 mg/g to 1,183.1 mg/g as the RPAC dosage increases from 250 mg to 1,500 mg.

The results of the ANOVA analysis indicate a significant difference in oil adsorption capacity between the dosage of 250 mg and other dosages. Therefore, the RPAC dosage of 250 mg was chosen as the optimal dosage for conducting experiments to investigate the effect of pH on the oil adsorption process of RPAC.

3.2.4. Effect of pH

The solution's pH significantly affects adsorption because it influences the adsorbent's surface properties and binding sites [42]. Moreover, changes in acidity or alkalinity in the oil solution can increase oil solubility, indicating a reduction in the oil's hydrophobicity. Consequently, this leads to a decrease in oil adsorption on the hydrophobic adsorbent surface, especially in highly acidic or alkaline solutions [37]. The investigation results regarding the impact of pH on the oil adsorption capacity and oil removal efficiency of RPAC are presented in Figure 13 within the pH range of 3 to 11.

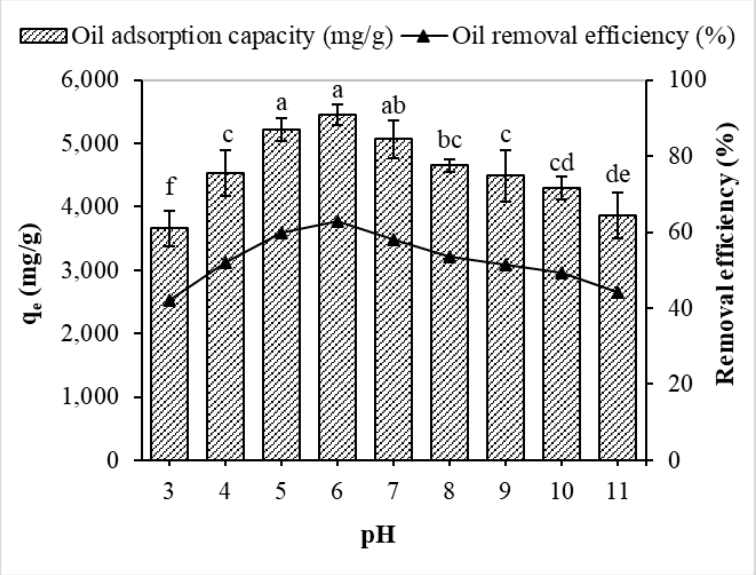

Figure 13. Effect of pH on oil adsorption capacity and removal efficiency (Experimental conditions: adsorbent particle size = 0.6 - 1.0, temperature = 25 ± 1°C, initial oil concentration = 1.0 % v/v, contact time = 60 min, adsorbent dosage = 250 mg per 250 ml of oil-contaminated water, and pH = 3 - 11). The error bars represent the mean (SD) for three replicates (n = 3).

Increasing the solution's pH from 3 to 6 enhances the oil adsorption capacity from 3,660.3 mg/g to 5,458.3 mg/g, increasing oil removal efficiency from 42.07% to 62.74%. At lower pH levels, the adsorbent's hydrophobic nature diminishes due to a considerable number of protons adsorbed on the adsorbent's surface [37]. Specifically, at lower pH (acidic conditions), there are many protons (H^+ ions) in the solution. These protons attach to the adsorbent's surface and neutralize its charged parts. This reduces the surface's ability to attract hydrophobic (water-repelling) molecules, making the biosorbent less hydrophobic and less effective at adsorbing such molecules. As the pH continues to rise, the oil adsorption capacity tends to decrease. Specifically, the oil adsorption capacity and removal efficiency drop to 3,859.0 mg/g and 44.36%, respectively, when the pH reaches 11. This phenomenon stems from pH's influence on the adsorbent's net charge and the oil surface. In an alkaline environment, protons are removed from charged functional groups on the surface of the adsorbent in the adsorption reaction mixture, thereby diminishing the overall positive charge and the affinity of the adsorption sites for negatively charged oil molecules [28]. In short, at acidic pH levels, the adsorbent surface carries a positive charge, which promotes the electrostatic attraction and subsequent adsorption of negatively charged contaminants (anions). In neutral pH conditions, the adsorbent surface charge approaches neutrality,

leading to adsorption through a combination of forces, including van der Waals interactions, hydrogen bonding, and electrostatic interactions. In alkaline environments, at high pH levels, adsorbent acquires a negative surface charge, allowing it to attract and adsorb positively charged contaminants (cations) through electrostatic interactions.

The ANOVA analysis results indicate no substantial difference in oil adsorption capacity among solution pH values of 5, 6, and 7. Nonetheless, a notable difference in oil adsorption capacity is observed between pH values of 5, 6, and 7 when compared to the pH values of the remaining solutions. Consequently, a solution pH of 6, demonstrating the most effective oil adsorption capacity, is selected as the optimal pH for the experimental optimization process. Other studies also show similar results, with optimal oil adsorption efficiency occurring within the neutral pH range. For instance, the research by [43], utilizing activated carbon derived from mango peels, determined an optimal pH of around 7.

3.3. Comparative analysis of oil adsorption capacity with other activated carbon materials

Several activated carbon materials sourced from different agricultural waste byproducts are compared with RPAC in this study by the author, and the results are presented in Table 6.

Table 6. Comparative analysis of oil adsorption capacity.

Materials	Method	Oil type	Maximum adsorption capacity	References
Barley Straw	Carbonized, 400 °C	Gas oil	8.5 - 9 g/g	[39]
Rice husks	Carbonized	Diesel oil	5.02 g/g	[44]
Rice husks	Carbonized	Diesel oil	2.78 g/g	[44]
Rice husks	Carbonized, 480 °C	Diesel oil	5.5 kg/kg	[45]
Coconut Coir	Carbonized, 600 °C	Crude oil	4,859.5 mg/g	[12]
RPAC	Carbonized, 550 °C	Diesel oil	5,712.0 mg/g	This study

Table 6 shows that the maximum adsorption capacity of RPAC in this study is higher than that of pyrolyzed rice husk reported in the research conducted by [44] and [45], as well as that of activated carbon from coconut coir [12]. However, compared to the findings [39], the maximum adsorption capacity of RPAC is lower than that of carbonized oat straw at 400°C for 0.5 to 3 hours. The activated carbon adsorbent derived from rambutan in this study excels in diesel adsorption compared to numerous activated carbon materials derived from agricultural by-products. This underscores the potential of RPAC as a highly effective oil absorbent for pollution remediation. Nevertheless, the treatment effectiveness of the adsorbent may vary depending on pyrolysis conditions, the type of tested oil, and the properties of the materials used in activated carbon production.

4. Conclusion

Activated carbon derived from rambutan peel demonstrated highly effective oil removal capabilities in water. The process involved carbonization and subsequent KOH activation, resulting in a more porous adsorbent with significantly increased surface area: 485.7680 (m^2/g) and 786.0143 (m^2/g), respectively. The pore volume also saw a substantial increase, going from 0.005293 to 0.05392 (cm^3/g), while the pore diameter expanded from 21.6 to 55.2 nm. Particularly noteworthy is the alkaline treatment, which generated larger and deeper pores, enhancing their abundance on the material's surface. Individual evaluations of factors influencing RPAC's oil removal efficiency and adsorption capacity identified optimal values. These include a 1% v/v oil concentration, a 60-minute contact time, a 250 mg adsorbent dosage, and a pH of 6. The adsorption process conformed well to the Langmuir isotherm model (R^2 = 0.9993), yielding a maximum adsorption capacity of 5,712.0 mg/g. Furthermore,

the pseudo-second-order model (R^2 = 0.9969) proved to be a more suitable fit for RPAC's oil adsorption process.

Author contribution statement: Defining and developing the research idea and researchframework: T.V.N., L.H.B.; Collecting data and literature, data analysis and synthesis: T.T.N., N.D.L.; Experimental research: T.T.N., N.D.L.; Drafting the manuscript: T.T.N.; Manuscript editing and revision: T.V.N., L.H.B.

Acknowledgement: We would like to express our gratitude for the support in terms of time, facilities, and financial resources provided by HUTECH University for conducting this study.

Competing interest statement: The authors declare that this article was the work of theauthors, has not been published elsewhere, has not been copied from previous research; therewas no conflict of interest within the author group.

Reference

1. ITOPF. *Tanker Spill Statistics 2021*; ITOPF Ltd, London, UK., 2022, 1–20.
2. Kolokoussis, P.; Karathanassi, V. Oil spill detection and mapping using Sentinel 2 imagery. *J. Mar. Sci. Eng.* **2018**, *6(1)*, 1–12.
3. Wardley-Smith, J. The control of oil pollution. Graham & Tortman Ltd, 1976.
4. Alaa El-Din, G.; Amer, A.A.; Malsh, G.; Hussein, M. Study on the use of banana peels for oil spill removal. *Alexandria Eng. J.* **2018**, *57(3)*, 2061–2068.
5. El-Nafaty, U.A.; Muhammad, I.M.; Abdulsalam, S. Biosorption and kinetic studies on oil removal from produced water using banana peel. *J. Civ. Eng. Res.* **2013**, *3(6)*, 125–136.
6. Idris, J.; Eyu, G.D.; Mansor, A.M.; Ahmad, Z.; Chukwuekezie, C.S. A preliminary study of biodegradable waste as sorbent material for oil-spill cleanup. *Sci. World J.* **2014**, *2014*, 1–5.
7. Lim, T.T.; Huang, X. Evaluation of Kapok (Ceiba Pentandra (L.) Gaertn.) as a natural hollow hydrophobic–oleophilic fibrous sorbent for oil spill cleanup. *Chemosphere* **2007**, *66(5)*, 955–963.
8. Banerjee, S.S.; Joshi, M.V.; Jayaram, R.V. Treatment of oil spill by sorption technique using fatty acid grafted sawdust. *Chemosphere* **2006**, *64(6)*, 1026–1031.
9. Kadirvelu, K.; Namasivayam, C. Activated carbon from coconut coirpith as metal adsorbent: Adsorption of Cd(II) from aqueous solution. *Adv. Environ. Res.* **2003**, *7(2)*, 471–478.
10. Maulion, R.V.; Abacan, S.A.; Allorde, G.G.; Umali, M.C.S. Oil spill adsorption capacity of activated carbon tablets from corncobs in simulated oil-water mixture. *Asia Pac. J. Multidiscip. Res.* **2015**, *3(5)*, 146–151.
11. Aljeboree, A.M.; Alshirifi, A.N.; Alkaim, A.F. Kinetics and equilibrium study for the adsorption of textile dyes on coconut shell activated carbon. *Arab. J. Chem.* **2017**, *10*, S3381–S3393.
12. Anwana Abel, U.; Rhoda Habor, G.; Innocent Oseribho, O. Adsorption studies of oil spill clean-up using coconut coir activated carbon (CCAC). *ASEAN J. Chem. Eng.* **2020**, *8(2)*, 36–47.
13. Atemkeng, C.D.; Anagho, G.S.; Tagne, R.F.T.; Amola, L.A.; Bopda, A.; Kamgaing, T. Optimization of 4-nonylphenol adsorption on activated carbons derived from safou seeds using response surface methodology. *Carbon Trends* **2021**, *4*, 100052.
14. Igwegbe, C.A.; Umembamalu, C.J.; Osuagwu, E.U.; Oba, S.N.; Emembolu, L.N. Studies on adsorption characteristics of corn cobs activated carbon for the removal of oil and grease from oil refinery desalter effluent in a downflow fixed bed adsorption equipment. *Eur. J. Sustain. Dev.* **2020**, *5(1)*, 1–14.
15. Sahu, J.N.; Agarwal, S.; Meikap, B.C.; Biswas, M.N. Performance of a modified multi-stage bubble column reactor for lead(ii) and biological oxygen demand

removal from wastewater using activated rice husk. *J. Hazard. Mater.* **2009**, *161(1)*, 317–324.
16. Angelova, D.; Uzunov, I.; Uzunova, S.; Gigova, A.; Minchev, L. Kinetics of oil and oil products adsorption by carbonized rice husks. *Chem. Eng. J.* **2011**, *172(1)*, 306–311.
17. Husseien, M.; Amer, A.; El- Maghraby, A.; Taha, N. Experimental investigation of thermal modification influence on sorption qualities of barley straw. *J. Appl. Sci. Res.* **2008**, *4(6)*, 652–657.
18. Huong, D. Agricultural by-products: Resources are being wasted. Government Electronic Newspaper, 2021. (in Vietnam)
19. Department of Horticulture. Handbook of farming techniques according to VietGAP for 10 major fruit trees. Ministry of Agriculture and Rural Development of Vietnam, 2022.
20. Oliveira, E.; Santos, J.; Goncalves, A.P.; Mattedi, S.; Jose, N. Characterization of the rambutan peel fiber (nephelium lappaceum) as a lignocellulosic material for technological applications. *Chem. Eng. Trans.* **2016**, *50*, 391–396.
21. Olga, V.R.; Darina, V.I.; Alexandr, A.I.; Alexandra, A.O. Cleanup of water surface from oil spills using natural sorbent materials. *Procedia Chemistry* **2014**, *10*, 145–150.
22. Al-Jammal, N.; Juzsakova, T. Review on the effectiveness of adsorbent materials in oil spills clean up. Proceedings of the 7th International Conference of ICEEE, Budapest, Hungary **2016**, 131–138.
23. Normah, N. et al. Hydrothermal carbonization of rambutan peel (*Nephelium lappaceum L.*) as a Green and low-cost adsorbent for Fe(II) removal from aqueous solutions. *Chem. Ecol.* **2022**, *38*, 1–17.
24. Ahmad, M.A.; Alrozi, R. Optimization of rambutan peel based activated carbon preparation conditions for remazol brilliant blue R removal. *Chem. Eng. J.* **2011**, *168(1)*, 280–285.
25. Omer, A.M.; Khalifa, R.E.; Tamer, T.M.; Ali, A.A.; Ammar, Y.A.; Mohy Eldin, M. S. Kinetic and thermodynamic studies for the sorptive removal of crude oil spills using a low-cost chitosan-poly (butyl acrylate) grafted copolymer. *Desalin. Water Treat.* **2020**, *192*, 213–225.
26. Kowanga, K.D.; Gatebe, E.; Mauti, G.O.; Mauti, E.M. Kinetic, sorption isotherms, pseudo-first-order model and pseudo-second-order model studies of cu(ii) and pb(ii) using defatted moringa oleifera seed powder. *J. Psychopharmacol.* **2016**, *5(2)*, 71–78.
27. Ho, Y.S.; McKay, G. Pseudo-second order model for sorption processes. *Process Biochem.* **1999**, *34(5)*, 451–465.
28. Nnamdi Ekwueme, B.; Anthony Ezema, C.; Asadu, C.O.; Elijah Onu, C.; Onah, T. O.; Sunday Ike, I.; Chinonyelum Orga, A. Isotherm modelling and optimization of oil layer removal from surface water by organic acid activated plantain peels fiber. *Arab. J. Chem.* **2023**, *16(2)*, 104443.
29. Ike, I.S.; Asadu, C.O.; Ezema, C.A.; Onah, T.O.; Ogbodo, N.O.; Godwin-Nwakwasi, E.U.; Onu, C.E. ANN-GA, ANFIS-GA and thermodynamics base modeling of crude oil removal from surface water using organic acid grafted banana pseudo stem fiber. *Appl. Surf. Sci.* **2022**, *9, 100259*.
30. Onu, C.E.; Nwabanne, J.T.; Ohale, P.E.; Asadu, C.O. Comparative analysis of RSM, ANN and ANFIS and the mechanistic modeling in eriochrome black-t dye adsorption using modified clay. *S. Afr. J. Chem. Eng.* **2021**, *36*, 24–42.
31. Hasanah, M.; Juleanti, N.; Priambodo, A.; Arsyad, F.; Lesbani, A.; Mohadi, R. Utilization of rambutan peel as s potential adsorbent for the adsorption of malachite

green, procion red, and congo red dyes. *Ecol. Eng. Environ. Technol.* **2022**, *23*, 148–157.

32. Njoku, V.O.; Foo, K.Y.; Asif, M.; Hameed, B.H. Preparation of activated carbons from rambutan (Nephelium lappaceum) peel by microwave-induced KOH activation for acid yellow 17 dye adsorption. *Chem. Eng. J.* **2014**, *250*, 198–204.
33. Aziz, A.; Mohamad Yusop M.F.; Ahmad, M.A. Removal of bisphenol S from aqueous solution using activated carbon derived from rambutan peel via microwave irradiation technique. *Sains Malays.* **2022**, *51(12)*, 3967–3980.
34. Tran, Q.T. et al. Experimental design, equilibrium modeling and kinetic studies on the adsorption of methylene blue by adsorbent: activated carbon from durian shell waste. *Materials (Basel)* **2022**, *15(23)*, 8566
35. Patmawati, Y.; Alwathan; Ramadani, N.H. Characterization of activated carbon prepare from low-rank coal of east kalimantan by using acid and base activation. Proceedings of the 8th Annual Southeast Asian International Seminar (ASAIS 2019) **2019**, 178–181.
36. Sokker, H.H.; El-Sawy, N.M.; Hassan, M.A.; El-Anadouli, B.E. Adsorption of crude oil from aqueous solution by hydrogel of chitosan based polyacrylamide prepared by radiation induced graft polymerization. *J. Hazard. Mater.* **2011**, *190(1)*, 359–365.
37. Cheu, S.C.; Kong, H.; Song, S.T.; Saman, N.; Johari, K.; Mat, H. High removal performance of dissolved oil from aqueous solution by sorption using fatty acid esterified pineapple leaves as novel sorbents. *RSC Adv.* **2016**, *6(17)*, 13710–13722.
38. Peng, D.; Lan, Z.; Guo, C.; Yang, C.; Dang, Z. Application of cellulase for the modification of corn stalk: leading to oil sorption. *Bioresour. Technol.* **2013**, *137*, 414–418.
39. Hussein, M.; Amer, A.A.; Sawsan, I.I. Oil spill sorption using carbonized pith bagasse: 1. preparation and characterization of carbonized pith bagasse. *J. Anal. Appl. Pyrolysis.* **2008**, *82(2)*, 205–211.
40. Tembhurkar, A.; Deshpande, R. Powdered activated lemon peels as adsorbent for removal of cutting oil from wastewater. *J. Hazard. Toxic Radioact. Waste* **2012**, *16(4)*, 311–315.
41. NwabuezeH, H.O.; Chiaha, P.N.; Ezekannagha, B.C.; Okoani, O.E. Acetylation of corn cobs using iodine catalyst, for oil spills remediation. *Int. J. Eng. Sci.* **2016**, *5(9)*, 53–59.
42. Wan Ngah, W.S.; Hanafiah, M.A.K.M. Adsorption of copper on rubber (hevea brasiliensis) leaf powder: kinetic, equilibrium and thermodynamic studies. *Biochem. Eng. J.* **2008**, *39(3)*, 521–530.
43. Olufemi, B.A.; Otolorin, F. Comparative adsorption of crude oil using mango (mangnifera indica) shell and mango shell activated carbon. *Environ. Eng. Res.* **2017**, *22(4)*, 384–392.
44. Vlaev, L.; Petkov, P.; Dimitrov, A.; Genieva, S. Cleanup of water polluted with crude oil or diesel fuel using rice husks ash. *J. Taiwan Inst. Chem. Eng.* **2011**, *42(6)*, 957–964.
45. Angelova, D.; Uzunova, S.; Uzunov, I.; Anchev, B. Dependence between oil sorption capacity of pyrolyzed rice husks and the composition and amount of fluids dispersed on their surface. *J. Chem. Technol. Metall.* **2012**, *47(2)*, 147–154.